Volume 13
Number 19
21 September 2025
Pages 5223-5572

Biomaterials Science

rsc.li/biomaterials-science

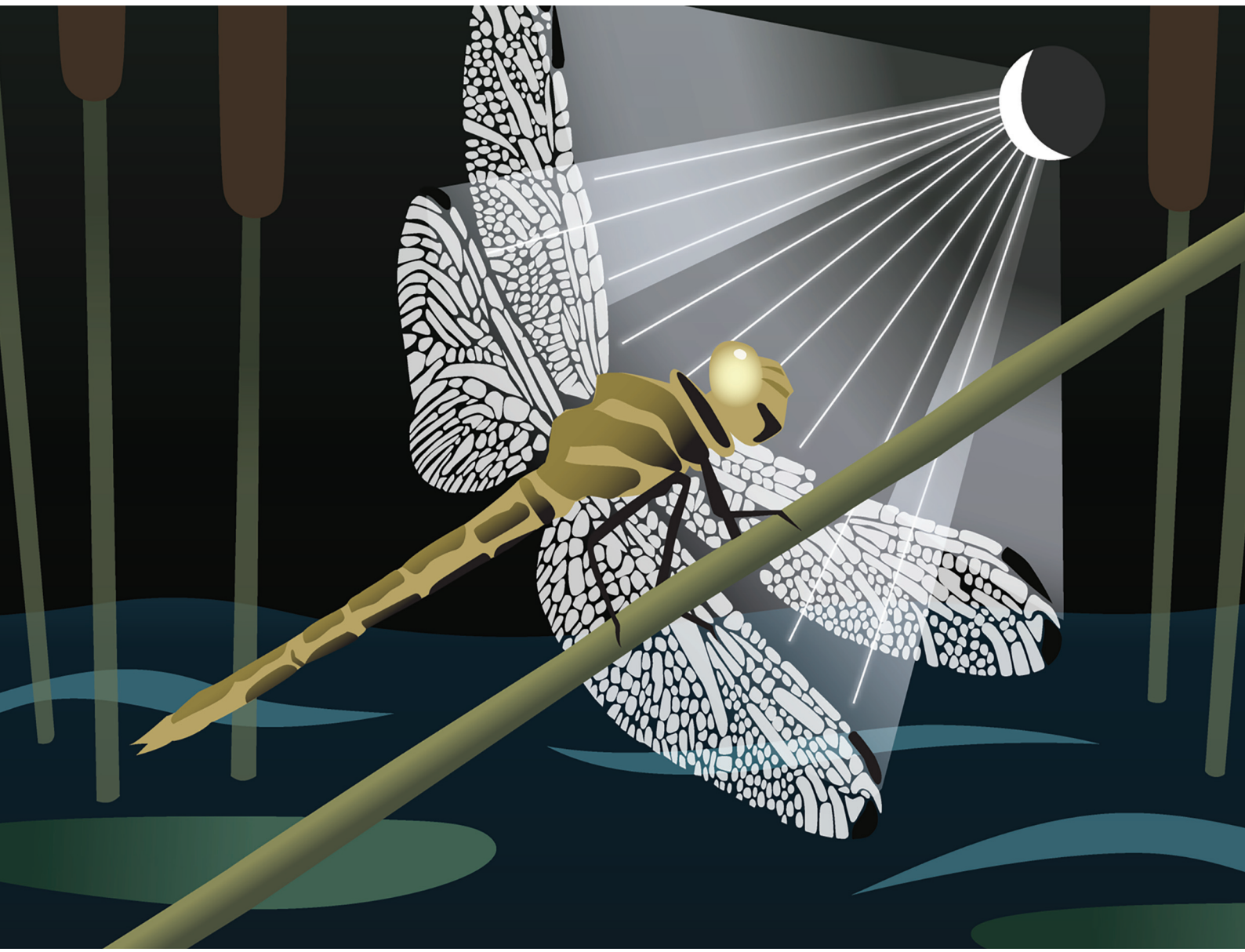

ISSN 2047-4849

ROYAL SOCIETY OF CHEMISTRY

PAPER
Anthony J. Convertine *et al.*
PISA printing perfusable microcapillaries

European Society for Biomaterials

Biomaterials Science

ROYAL SOCIETY OF CHEMISTRY

PAPER

View Article Online
View Journal | View Issue

Cite this: *Biomater. Sci.*, 2025, **13**, 5358

PISA printing perfusable microcapillaries†

Aaron Priester,[a] Jimmy Yeng,[a] Yuwei Zhang,[b] David Christofferson,[a] Risheng Wang [b] and Anthony J. Convertine *[a]

Received 10th April 2025,
Accepted 19th May 2025

DOI: 10.1039/d5bm00547g

rsc.li/biomaterials-science

Polymerization-induced self-assembly (PISA) printing combines reversible addition–fragmentation chain transfer (RAFT) polymerization with digital light projection (DLP) photolithography to create high-resolution three-dimensional structures without permanent covalent crosslinks. Here, we intoduce a simplified, one-pot, purification-free synthesis for multi-chain transfer agent (multi-CTA) scaffolds that spontaneously form robust physical networks durnig printing, stabilized by interparticle bridges and knots. By tuning solvent-resin chemistry and polymer composition, we achieved precise control over nanoscale morphologies and selective distribution behaviors. This approach was demonstrate through successful fabrication of perfusable microvascular networks and open-channel polydimethylsiloxane (PDMS) microfluidic devices, where sacrificial scaffolds dissolved cleanly to yield stable microchannels. Collectively, these findings enhance the accessibliity, flexibility, and functionality of PISA printing, offering an efficient and adaptable platform for microfabrication, rapid prototyping, and advance d tissue engineering applications.

Introduction

Bioprinting has emerged as a transformative tool in tissue engineering and regenerative medicine, enabling the fabrication of three-dimensional cellular constructs with defined architectures.[1] Despite many advances, current bioprinting strategies face challenges related to speed, material properties, and balancing structural fidelity with cell viability.[2] Extrusion-based methods, for example, mechanically deposit bioinks through fine nozzles in a slow, point-by-point manner, subjecting encapsulated cells to shear stress while limiting throughput and scale.[3] While narrower nozzles improve resolution, they lower cell viability; conversely, larger nozzles enhance cell survival at the expense of fine detail.[3] These trade-offs have prompted the search for approaches that produce stable, high-resolution constructs without compromising printing speed or cell health.

Digital light processing (DLP) photolithography offers a faster alternative by curing entire layers simultaneously rather than depositing them incrementally.[4,5,17,18] This approach enables high-resolution structures with greater speed and precision.[5,17] However, typical DLP resins contain multifunctional monomers that form permanently crosslinked polymer networks, yielding mechanically stable but insoluble materials.[4,5,18] In many tissue engineering applications, the ability to dissolve or reconfigure a material after printing is desirable.[5,18] Balancing robust structural formation with post-print flexibility requires a new class of photopatternable yet reversibly assembled materials.[19]

Polymerization-induced self-assembly (PISA) provides a means to achieve this balance.[6,7,20] Under reversible addition–fragmentation chain transfer (RAFT) conditions, PISA grows a solvophobic block from a solvophilic block, leading to spontaneous self-assembly into amphiphilic copolymers.[6,7,21] Traditional RAFT-based PISA typically relies on monofunctional chain transfer agents (CTAs), producing soluble nano-objects or weak gels.[8,9,28,29] While highly tunable, these weaker assemblies lack the mechanical robustness needed for three-dimensional objects.[22,30] To address this shortcoming, PISA Printing merges RAFT-mediated PISA with DLP photolithography to generate physically crosslinked networks *via* multi-CTA functional scaffolds.[10,23–25] Traditional RAFT-based DLP resins rely on the formation permanent covalent crosslinks which limit their useful in certain applications, though the 'living' nature of RAFT does enable post-printing modifications of these materials.[20,23] Unlike conventional DLP resins, which rely on these permanent covalent crosslinks, multi-CTA scaffolds form physically crosslinked networks that remain soluble in suitable solvents.[10–12,19,20] This enables the fabrication of complex, high-resolution parts that can later be selectively dissolved or adjusted, bridging a key gap in current bioprinting methods.[10–12,26]

Recently, we introduced PISA Printing as a method for fabricating dissolvable and mechanically robust structures using

[a]*Department of Materials Science and Engineering, Missouri University of Science and Technology, 1400 North Bishop Avenue, Rolla, MO 65409, USA. E-mail: convertinea@mst.edu*
[b]*Department of Chemistry, Missouri University of Science and Technology, 400 W 11th Street, Rolla, MO 65409, USA*

† Electronic supplementary information (ESI) available. See DOI: https://doi.org/10.1039/d5bm00547g

RAFT-mediated self-assembly combined with photolithography.[10] In prior work, we explored how graft density, polymer composition, and self-assembly pathways affect the mechanical strength and dissolution rates of PISA-printed structures.[11,12] A key advancement was incorporating acrylamide (AM) as a phase-separating monomer in isopropanol, with dissolution rates adjusted by *N*-(butoxymethyl)acrylamide (BAM).[11] This approach enabled the fabrication of dissolvable microneedles with tunable kinetics, as well as high-resolution structures suitable for a variety of biomedical applications.[11,12] By varying the AM-to-BAM ratio, dissolution profiles could be systematically controlled while preserving print fidelity.[11] These findings demonstrate that RAFT PISA can yield materials stable during fabrication yet dissolvable under physiological or otherwise appropriate conditions.[10–12,27]

A major challenge in tissue engineering remains the fabrication of functional microvasculature to support cell viability in thick constructs.[13,14] Engineered tissues quickly develop necrotic cores without a perfusable capillary network, necessitating methods that can reliably produce microvascular structures.[13,15,16,31–33] Traditional extrusion and DLP printing struggle to achieve dense, perfusable capillaries at the necessary scale.[14,32,33] One widely used strategy involves sacrificial templating, in which a fugitive ink is printed to outline the desired channel structure and later removed to create open vessels.[15,16,31,33] This technique has successfully enabled microfluidic and vascular network fabrication, but it requires additional steps and careful compatibility between the sacrificial material and the surrounding matrix.[16,31,33]

PISA Printing offers an alternative route to perfusable microcapillary structures without the need for an additional sacrificial filler.[10–12,24–26] In this study, we extend the versatility of PISA Printing by demonstrating the use of three monomers with distinct self-assembly and dissolution characteristics. Acrylamide self-assembles in ethanol and dissolves rapidly in water, with rates further controlled by BAM content.[11] Isobornyl acrylate (IBA) also self-assembles in ethanol but dissolves in non-polar solvents, while diacetone acrylamide (DAAM) undergoes PISA in water and dissolves in polar organic solvents. By combining these monomers and leveraging their unique solubility profiles, we fabricate complex, multi-material structures with precise, selective dissolution. These results broaden the range of applications for PISA Printing, opening new possibilities for dynamic materials in advanced tissue engineering, perfusable microcapillary networks, and microfluidic device fabrication.[10–12,24,25,32]

Experimental section

Materials

N,*N*-Dimethylacrylamide (DMA, >99%), *N*-(2-hydroxyethyl) acrylamide (HEAm, >98%), diacetone acrylamide (DAAm, >98%), acrylamide (AM, >98%), diphenyl(2,4,6-trimethylbenzoyl)phosphine oxide (TPO, >98%), methylene bisacrylamide (MBAC, >98%) and isobornyl acrylate (IBA, >90%) were sourced from TCI America. 4-((((2-Carboxyethyl)thio)carbonothioyl)thio)-4-cyanopentanoic acid (CCC, 95%) was obtained from Boron Molecular. 4,4′-Azobis(4-cyanovaleric acid) (ABCVA, >75%) and phenol red (~95%) were sourced from Sigma-Aldrich. Vinyl-terminated polydimethylsiloxane 100 cSt (divinyl-PDMS) and [4–6%] (mercaptopropyl)methylsiloxane – dimethylsiloxane copolymer 120–170 cSt (thiolated-PDMS) were both obtained from Gelest. All solvents, including ethanol, dimethyl sulfoxide (DMSO), tetrahydrofuran (THF), and butyl acetate were sourced from TCI. Aqueous dyes including crystal violet, Direct Red 1, and fluorescein disodium salt, gelatin (type B, bovine skin) and methacrylic anhydride (>98%) were obtained from Sigma-Aldrich.

Instrumentation and equipment

Atomic force microscopy (AFM) was conducted using a Dimension Icon system (Bruker) operating in ScanAsyst air mode at a scan rate of 0.996 Hz. HQ:NSC14/Cr–Au BS probes (Nanoandmore) with a resonance frequency of 160 kHz and nominal spring constant of 5 N m^{-1} were used for AFM imaging. Digital light processing (DLP) 3D printing was performed using a Phrozen Sonic Mini 8KS printer (405 nm light, 3 mW cm^{-2}). UV curing for PDMS resins was conducted using a handheld 30 W, 405 nm UV lamp Gelatin methacrylate (GelMA) was synthesized in-house, with detailed procedures described separately.

Synthesis of multi-CTA functional polymer scaffolds

Multi-CTA polymer scaffolds were synthesized using reversible addition–fragmentation chain transfer (RAFT) copolymerization. In a typical reaction, DMA (15.0 g, 151 mmol), CCC (0.465 g, 1.51 mmol), and MBAC (0.163 g, 1.06 mmol) were dissolved in a 50 mL round-bottom flask. ABCVA (21 mg, 75.6 μmol) was added, followed by distilled water (15 g) to achieve a final monomer concentration of 50 wt%. The solution was degassed by purging with argon for 30 minutes and polymerized at 60 °C in a preheated water bath for 24 hours. Conversion was confirmed *via* ^{1}H NMR spectroscopy, and the resulting scaffolds were used without further purification. For ethanol-based synthesis, identical experimental conditions were used, replacing water with ethanol.

Synthesis and purification of gelatin methacrylate (GelMA)

Gelatin methacrylate (GelMA) was synthesized using type B gelatin from bovine skin. Briefly, 10 g of gelatin was dissolved in 90 mL of pre-heated 1× phosphate-buffered saline (PBS) at 50 °C under continuous magnetic stirring for approximately 30 minutes until fully dissolved. Subsequently, 6 g (38.9 mmol) of methacrylic anhydride at room temperature was slowly added to the gelatin solution in 1 mL increments over 10 minutes. The reaction was allowed to proceed at 50 °C for an additional 3 hours with constant stirring. After completion, the reaction mixture was centrifuged at 3000 rpm for 15 minutes, and the supernatant containing crude GelMA was collected.

The crude GelMA solution was then purified through dialysis using regenerated cellulose dialysis tubing with a molecular weight cutoff of 12–14 kDa. Dialysis was initially performed against 1× PBS at 40 °C for 2 days, followed by dialysis against distilled water at 40 °C for an additional five days. Finally, the dialyzed GelMA solution was freeze-dried to obtain the purified GelMA product.

PISA printing with acrylamide and hydroxyethyl acrylamide

A resin formulation was prepared with a 50/50 molar ratio of acrylamide (AM) and *N*-(2-hydroxyethyl)acrylamide (HEAM), using a monomer-to-CTA ratio of 500 (250 equivalents each of AM and HEAM). The resin contained 40 wt% total solids, defined as the combined mass of polymer and monomers in ethanol solution. TPO (0.85 wt% relative to total solids) was used as the photoinitiator, while phenol red (0.02 wt%) was included as a photoabsorber. A representative procedure is as follows: to a 100 mL beaker, 5 g one pot polymer in EtOH (2.5 g polymer, 0.252 mmol CCC), 4.48 g of AM (63.0 mmol), 7.24 g of HEAM (63.0 mmol) and 18.83 g of ethanol were added. The solution was placed on a stir plate until homogenous. 121 mg of TPO (0.347 mmol, 0.85 wt% with respect to solids) were added and dissolved. Lastly, 0.568 g of a 5 mg g^{-1} solution of phenol red in DMSO (2.84 mg, 0.02 wt% with respects to solids) was dripped into the resin and stirred until homogeneous (~10 minutes). Printing was performed with a layer thickness of 50 μm and exposure times ranging from 60 to 70 seconds.

PISA printing with isobornyl acrylate (IBA)

A resin based on isobornyl acrylate (IBA) was prepared with a monomer-to-CTA molar ratio ([M]/[CTA]) of 125 and formulated at 40 wt% total solids. In a representative preparation, ethanol-based one-pot polymer solution (5 g, containing 2.5 g polymer, 0.252 mmol CCC), IBA monomer (6.56 g, 31.5 mmol), distilled water (1.36 g), and ethanol (9.73 g) were combined and stirred until homogeneous. Subsequently, TPO photoinitiator (77.0 mg, 0.221 mmol, corresponding to 0.85 wt% with respect to solids) was added and dissolved. 0.227 g of a 5 mg g^{-1} solution of phenol red in DMSO (1.14 mg, 0.02 wt% with respects to solids) was incorporated, and the resin was stirred for 10 minutes before printing. Printing was conducted with exposure times of 90–100 s per layer and layer thicknesses of 35 μm.

PISA printing with diacetone acrylamide (DAAM)

A DAAM-based resin was formulated with an initial monomer-to-CTA molar ratio ([M]/[CTA]) of 250 and prepared at a total solids concentration of 40 wt%. In a representative preparation, aqueous one-pot polymer solution (5 g, containing 2.5 g polymer, 0.252 mmol CCC), DAAM monomer (10.66 g, 63 mmol), and distilled water (17.24 g) were combined and stirred until homogeneous. Subsequently, lithium phenyl-2,4,6-trimethylbenzoylphosphinate (LAP, 111 mg, 0.321 mmol, corresponding to 0.85 wt% with respect to solids) was added and dissolved. 0.527 g of a 5 mg g^{-1} solution of phenol red in DMSO (2.63 mg, 0.02 wt% with respects to solids) was incorporated, and the resin was stirred for 10 minutes before printing. Printing was conducted with exposure times of 15–30 s per layer. LAP was synthesized as described elsewhere.[31]

Dissolution and selective removal studies

Multi-material prints consisting of cylinders and dragonflies were fabricated using AM/HEAM, IBA, and DAAM-based resins. To fabricate the parts for these studies, IBA-based dragonflies were printed atop AM/HEAM cylinders, AM/HEAM-based dragonflies were printed atop IBA-based cylinders, and DAAM-based dragonflies atop IBA-based cylinders. Dissolution testing was conducted by immersing composite parts in solvents selectively dissolving each material: AM/HEAM dragonflies in water, DAAM dragonflies in ethanol, and IBA dragonflies in THF. Dissolution times varied, with AM/HEAM dissolving within 30 minutes, DAAM in approximately 2 hours, and IBA requiring overnight immersion.

Fabrication of perfusable capillary networks

A three-layer CAD design approach was used to fabricate capillary structures, with the middle layer selectively dissolved post-printing to create open channels between two crosslinked layers. Perfusion was validated using aqueous dyes (Direct Red 1, crystal violet, fluorescein disodium salt). For this approach, a chemically-crosslinkable resin based on HEAM + 1 wt% MBAC (40 wt% solids in EtOH) was printed as the first layer. This was followed by printing an AM/HEAM PISA-based vasculature layer next before finally switching back to the HEAM/MBAC crosslinkable resin for the final layer. The idea is that the third layer will overcure to the base layer, fully encapsulating the areas around and between the vasculature. Following printing, the parts were submerged in distilled water, dissolving out exposed areas of the AM/HEAM vasculature and leaving behind hollow channels. Aqueous solutions of the dyes were then injected through the parts for perfusability studies. Parts were printed on the Phrozen Sonic Mini 8KS using a normal layer exposure of 70 s per layer and layer thicknesses of 50 μm.

An alternative approach embedded DAAM-printed filaments within a GelMA hydrogel, followed by selective dissolution in heated DMSO to yield open microfluidic networks. In this approach, vasculature CAD designs were printed directly onto the build plate using DAAM resin printing conditions. Molds for the vasculature were DLP-printed using AnyCubic commercially available resin. Vasculature parts were submerged into either a PDMS-based resin (33 wt% divinyl PDMS, 67 wt% thiolated-PDMS, 1 wt% TPO at 60% solids in butyl acetate) or a GelMA-based resin (10 wt% in distilled water with 1 wt% LAP). The ends of the vasculature were kept out of the resin (non-submerged) so they could be dissolved out following curing. Resins were cured under UV light using a 405 nm 30W lamp for 30 seconds, removed from the mold and post-cured an additional 30 seconds. Parts were submerged in heated DMSO (50 °C) for one day, followed by dialysis against water to remove all DMSO prior to the injection of aqueous dye solutions.

Fabrication of PDMS-based microfluidic devices

PDMS matrices with open cylindrical channels were fabricated by casting a PDMS thiol–ene resin over printed sacrificial molds, followed by UV curing and selective dissolution of the printed molds in water overnight. In this study, CAD designs of cylinders with a surrounding wall were printed directly on the build plate using AM/HEAM-based resins. To ensure no failures, exposure times for these prints were increased to 100 s with layer thicknesses still fixed at 50 μm. Following printing, a PDMS-based resin (33 wt% divinyl PDMS, 67 wt% thiolated-PDMS, 1 wt% TPO at 60% solids in methyl ethyl ketone (MEK)) was cast into the cylinder molds directly onto the build plate. Resins were cured for approximately 1 minute using a 405 nm 30 W lamp at a distance of 1 cm. Following curing, the plate was submerged in distilled water, allowing the AM/HEAM cylinders and walls to be removed by dissolution. This left behind PDMS-based parts with hollow cylindrical channels in the part. These channel diameters ranged from 128 to 497 μm as will be discussed in the results section.

Resolution and overcuring analysis

To determine an optimal amount of photoabsorber need to produce vasculature with high resolution and small feature sizes, studies were run by varying the photoabsorber concentration in DAAM-based PISA resins using either 0, 0.005, 0.01 or 0.025 wt% phenol red photoabsorber with respect to solids. Blood vessel CAD files were printed at a fixed size to observe how much overcure occurred during printing. Prints were imaged along with a reference for scale using a light microscope. ImageJ software was used to determine the degree of overcuring in the blood vessel parts using the known scale reference. Additionally, once an optimal amount of photoabsorber was determined, this resin was then used to print the vessel at various sizes to determine how small in scale features could be printed. Results of these studies are shown in ESI Fig. 1.†

Atomic force microscopy (AFM) characterization

To prepare the samples, 10 μL of DAAM or IBA-based PISA resins were applied onto a freshly cleaved mica surface. The resin was then exposed to UV light for 1 minute to initiate the self-assembly process. Following this, the samples were allowed to be dried in air for 60 minutes. The resulting deposited samples were subsequently examined using Atomic Force Microscopy (AFM) (Dimension Icon system, Bruker), operating in Scanasyst air mode with a scan rate of 0.996 Hz. HQ:NSC14/Cr–Au BS probes purchased from Nanoandmore, featuring a resonance frequency of 160 kHz and a nominal spring constant of 5 N m^{-1}, were used in this analysis.

Results and discussion

Fig. 1 illustrates key differences between conventional photolithography, RAFT-mediated polymerization-induced self-assembly (PISA), and our newly developed multi-CTA PISA Printing approach. Conventional photolithographic resins (Fig. 1A) consist of multifunctional monomers (blue and red circles containing multiple vinyl groups). These monomers polymerize under UV light to form rigid, insoluble polymer networks through covalent crosslinking. While this method ensures excellent mechanical strength and precise structural fidelity, the permanent covalent bonds prevent subsequent modification or reshaping.

In comparison, traditional RAFT-mediated PISA (Fig. 1B) employs monofunctional macro-chain transfer agents (macro-CTAs), represented by blue polymer chains with a single yellow CTA group. These macro-CTAs guide the self-assembly of monomers into diverse nano-objects, such as spheres, worms, or vesicles (red structures). The nano-objects formed in this process rely mainly on noncovalent interactions for stability, providing excellent tunability and easy dissolution, but often lacking mechanical strength.

Our multi-CTA PISA Printing method (Fig. 1C) combines the strengths of both techniques. Here, polymers contain multiple CTA groups (blue polymer chains with multiple yellow CTA functionalities), enabling the formation of physically crosslinked gels during PISA. These gels achieve a balance between structural durability and ease of post-processing adjustments. We hypothesize that physical crosslinking in these gels primarily arises through two mechanisms: interparticle bridging (Fig. 1D), in which polymer chains are proposed to physically link separate assembled domains (red), and interparticle knotting (Fig. 1E), involving the hypothesized entanglement of stabilizing corona segments (blue and green polymer chains) across these domains. Although we have not directly visualized interparticle bridging or knotting at the molecular level due to experimental limitations, atomic force microscopy (AFM) images (Fig. 4) clearly demonstrate distinct, well-defined polymerization-induced self-assembly (PISA) morphologies, strongly indicative of physical network formation. Our previous studies further support these hypotheses, as monofunctional scaffolds bearing only a single RAFT agent per polymer chain do not form mechanically robust printed parts under identical conditions, underscoring the necessity of multi-CTA scaffolds to achieve mechanical integrity through the proposed mechanisms. This dual physical-crosslinking mechanism imparts mechanical integrity similar to that of conventional photolithography while maintaining the ability to reversibly assemble and disassemble the material. This reversibility enables controlled dissolution and flexible post-fabrication adjustments, addressing limitations associated with conventional photolithographic and traditional PISA approaches.

Previously, we reported the development and application of multi-CTA functional scaffolds (MCFS) for polymerization-induced self-assembly (PISA) printing, a methodology combining RAFT-mediated polymerization with photolithography [10–12]. Unlike conventional RAFT PISA methods, which typically utilize monofunctional macro-chain transfer agents (macro-CTAs) and yield soluble nanostructures or mechanically weak gels, our earlier studies introduced polymer

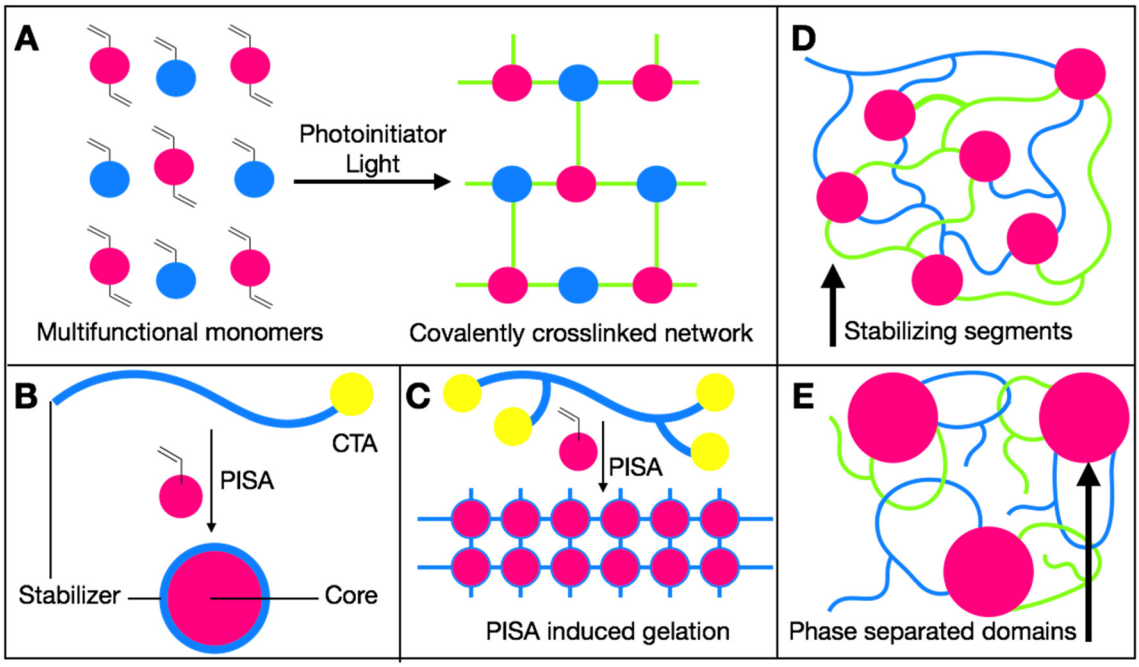

Fig. 1 Schematic representations comparing conventional photolithography, typical RAFT PISA, and multi-CTA PISA printing. (A) Conventional photolithographic resins composed of multifunctional monomers (depicted as blue and red circles containing multiple vinyl groups) form insoluble, covalently crosslinked polymer networks upon exposure to light in the presence of a photoinitiator. (B) Typical RAFT polymerization-induced self-assembly (PISA) using monofunctional macro-chain transfer agents (macro-CTAs; blue chains terminated by a single yellow CTA) as stabilizing segments. Under suitable monomer-solvent conditions, polymerization induces spontaneous formation of nano-objects such as spheres, worms, and vesicles (red). (C) Multi-CTA functionalized scaffolds (blue chains with multiple yellow CTA groups) undergoing PISA form physically crosslinked gels. This physical crosslinking occurs through two hypothesized mechanisms: (D) Interparticle bridges between distinct phase-separated domains (red), connecting individual polymer particles, and (E) interparticle knots formed by entanglements of the stabilizing corona segments (blue and green chains) linking the phase-separated domains (red).

scaffolds bearing multiple CTA groups. This multi-CTA architecture facilitated the formation of physically crosslinked gels with improved mechanical properties due to enhanced interparticle bridging and knot formation between phase-separated domains. However, the previously described synthesis of MCFS involved multi-step procedures and extensive purification, potentially limiting broader applicability.

To simplify this process and improve accessibility, we developed a one-pot, purification-free synthetic method employing only commercially available reagents. As depicted in Fig. 2, this synthetic approach involves RAFT copolymerization of *N*,*N*-dimethylacrylamide (DMA) with a small fraction of methylene bisacrylamide (MBAC) in either aqueous or ethanolic media. Polymerization is typically conducted at an initial monomer : CTA : bisacrylamide molar ratio of 100 : 1 : 0.7, achieving quantitative conversion within approximately 18 hours. Under these optimized conditions, soluble and branched MCFS (illustrated as blue polymer chains bearing multiple CTA groups, indicated by yellow circles) are obtained directly, without the need for additional purification or conjugation reactions. Increasing the bisacrylamide content beyond this optimal ratio results in highly crosslinked, insoluble gels rather than soluble polymer scaffolds, underscoring the importance of this optimized formulation.

Additionally, Fig. 2 illustrates three monomer systems employed in our PISA printing studies, selected based on their distinct solubility and self-assembly properties. Diacetone acrylamide (DAAM) undergoes PISA in water and dissolves readily in polar organic solvents; acrylamide/2-hydroxyethyl acrylamide (AM/HEAM) undergoes PISA in ethanol and is soluble in water; and isobornyl acrylate (IBA) undergoes PISA in ethanol but dissolves selectively in some non-polar organic solvents such as THF and dioxane. By choosing these complementary monomers, we fabricated multi-material structures with precisely controlled dissolution behaviors.

Beyond the use of pure monomer systems, copolymerization approaches were also implemented to further modulate mechanical and dissolution properties. Incorporating acrylamide (HEAM) into acrylamide-based formulations reduced brittleness and mitigated cracking of printed parts. Additionally, previous work demonstrated that including hydrophobic *N*-(butoxymethyl)acrylamide (BAM) into acrylamide-based resins allowed precise tuning of aqueous dissolution kinetics.[11] Increasing the proportion of BAM systematically reduced dissolution rates, providing concentration-dependent control over degradation behavior in PISA-printed materials.

Following the establishment of our simplified, one-pot synthesis of MCFS, we evaluated their practical applicability

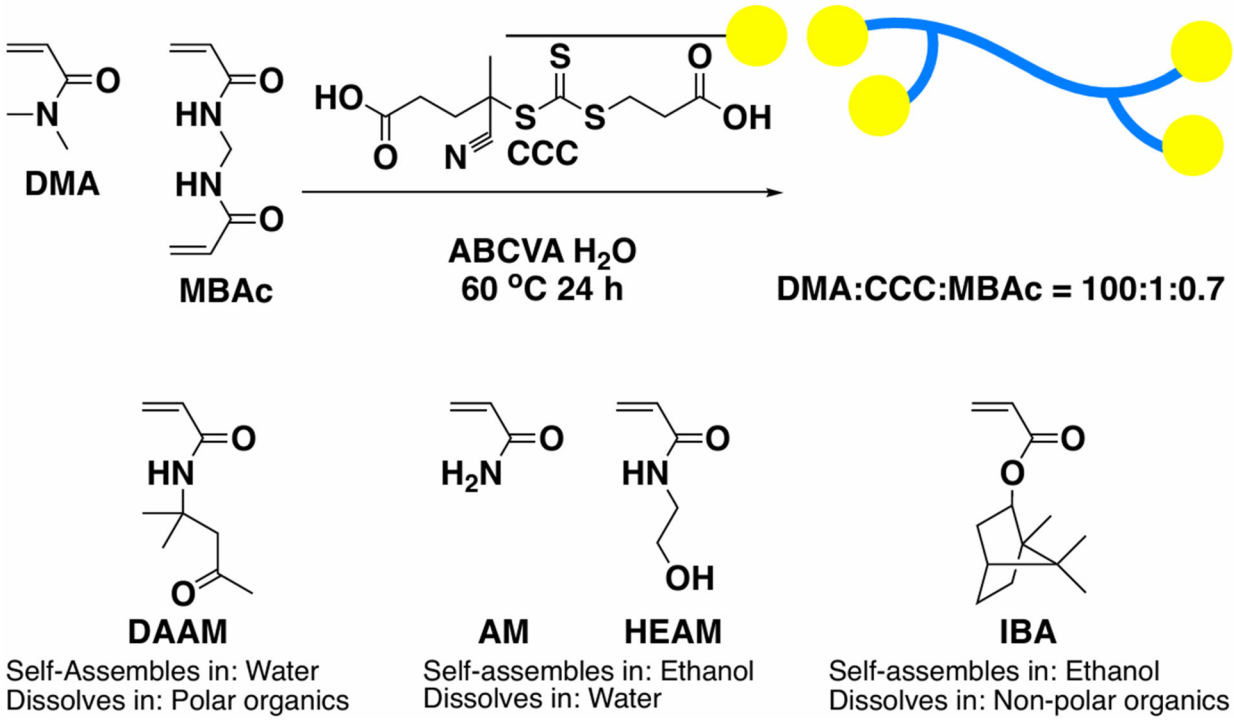

Fig. 2 Schematic illustration of a simplified one-pot synthesis of multi-CTA functional scaffolds (MCFS) designed for PISA printing. MCFS are synthesized *via* RAFT copolymerization of *N*,*N*-dimethylacrylamide (DMA) with a small quantity of methylene bisacrylamide (MBAC) in aqueous or ethanolic media. The resulting MCFS, depicted as blue polymer chains containing multiple CTA functionalities (represented by yellow circles), can be directly employed without additional purification. Typical polymerization conditions involve a molar ratio of monomer : CTA : bisacrylamide at 100 : 1 : 0.7, yielding soluble, branched polymers rather than insoluble gels, which form at higher crosslinker ratios. Additionally, three distinct monomer systems explored in this study are presented: diacetone acrylamide (DAAM), polymerized *via* PISA in water and soluble in polar organic solvents; acrylamide (AM) and hydroxyethyl acrylamide (HEAM), polymerized *via* PISA in ethanol and soluble in water; and isobornyl acrylate (IBA), polymerized *via* PISA in ethanol and soluble in non-polar organic solvents. Further modulation of the printed structures' mechanical and dissolution characteristics can be achieved by varying the monomer compositions and employing specific copolymerization strategies.

through multi-material printing experiments and resolution optimization studies, as depicted in Fig. 3. The left panel demonstrates multi-material prints consisting of cylindrical bases and dragonfly-shaped structures, fabricated from distinct resin formulations with tailored dissolution properties. Cylindrical bases shown in the images from left to right were printed from IBA, IBA, and AM/HEAM, respectively, while the corresponding dragonfly-shaped features were printed from AM-*co*-HEAm (left), DAAm (center), and IBA (right). Immersing these multi-material prints into selective solvents resulted in precisely controlled dissolution. On the far left panel, AM-*co*-HEAm dragonflies dissolved selectively in water over time when moving down the panel, leaving the IBA base intact. Here the dragonfly can be observed dissolving midway through the dissolution process in water (left panel, middle image). Similarly, in the middle panel, DAAm dragonflies dissolved selectively over time in ethanol as you move down the panel, also preserving their IBA bases. This dragonfly can also be observed midway through its dissolution process in ethanol (middle panel, middle image). Lastly, on the right panel, IBA dragonflies dissolved selectively in THF over time as you move down the panel, preserving the underlying AM/HEAM base. Again, this dragonfly can also be observed midway through its dissolution process in THF (right panel, middle image). These results illustrate how strategic monomer selection facilitates the fabrication of intricate multi-material structures with tailored and predictable dissolution behaviors.

After developing our streamlined one-pot synthesis of MCFS, we explored their practical use in multi-material printing trials and resolution optimization, as shown in Fig. 3. In the left panel, cylindrical bases and dragonfly-shaped structures were printed from different resin formulations designed for selective dissolution. The bases, moving from left to right, were fabricated using IBA, IBA, and AM/HEAM, while the dragonflies were made from AM-*co*-HEAm (left), DAAm (center), and IBA (right). Immersion in specific solvents produced precise, targeted dissolution: AM-*co*-HEAm dissolved in water and left the IBA base intact; DAAm dissolved in ethanol and preserved the IBA base; and IBA dissolved in THF, preserving the AM/HEAM base. These outcomes show that an appropriate selection of monomers allows the creation of detailed, multi-material structures with predictable dissolution.

The right panel of Fig. 3 highlights the structural fidelity achieved using DAAM and AM/HEAM formulations. Capillary structures printed from these resins underwent systematic evaluation to determine how photoabsorber content influ-

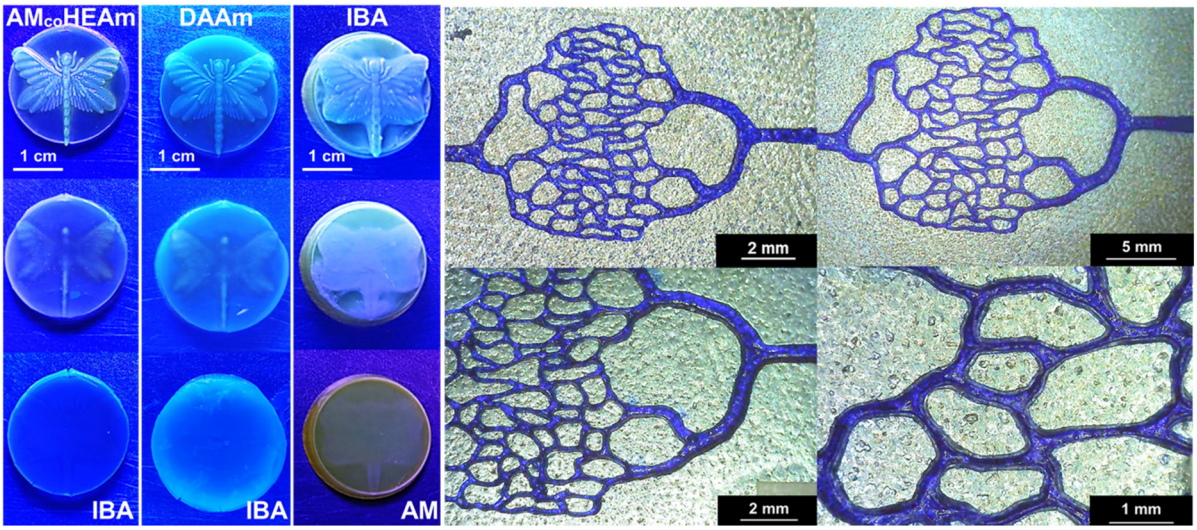

Fig. 3 Illustration of multi-material PISA printing and resolution optimization. (Left) Multi-material objects composed of cylindrical bases and dragonfly-like features printed from tailored resin compositions. From left to right, the bases are IBA, IBA, and AM/HEAM, while the dragonflies are AM-*co*-HEAm, DAAm, and IBA. Immersion in specialized solvents removes each dragonfly without affecting the base: AM-*co*-HEAm dissolves in water, DAAm in ethanol, and IBA in THF. Each dragonfly can be observed midway through its dissolution process for its respective composition and solvent, as represented by the middle image in each panel of these studies. (Right) This panel shows the resolution enhancements possible with AM-*co*-HEAm-based resins. Printed capillary structures were used to assess the effects of photoabsorber concentration on printing precision. Reducing unwanted curing led to accurate, reproducible microvascular architectures. Scale bars indicate feature size.

enced resolution and shape retention. Data in ESI Fig. 1† show that incorporating phenol red at 0.025 wt% reduced overcure to less than 30%, yielding fine-resolution features. By controlling unnecessary curing, we obtained reproducible, high-resolution microvascular elements, illustrated in the figure. The scale bars provide dimensional context.

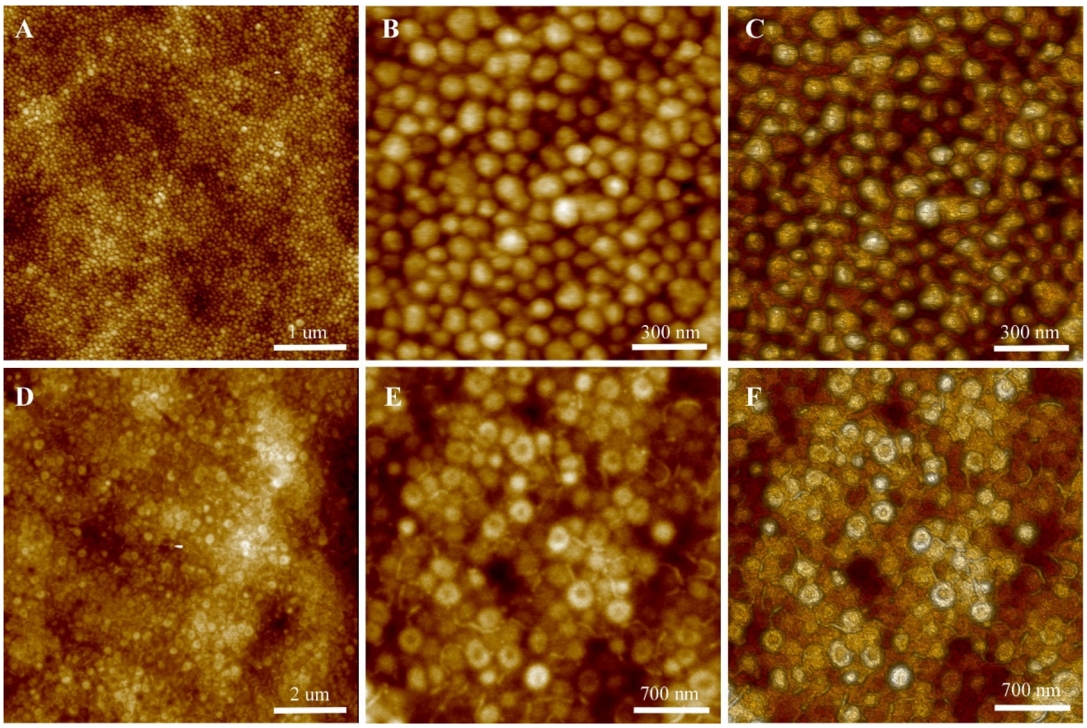

Fig. 4 Representative AFM images of nanostructures formed *via* PISA using DAAm-based (top row) and IBA-based (bottom row) resins. Panels A–C depict well-defined spherical domains from DAAm resins at increasing magnifications. Panels D–F illustrate vesicle-like morphologies from an IBA resin at DP 500 and 45 wt% solids, which did not produce stable 3D parts under the same curing conditions. All samples were briefly irradiated with UV light and air-dried prior to imaging. Scale bars provide dimensional reference.

To further explore the nano-scale morphologies achievable *via* photopolymerization-induced self-assembly (PISA), we performed AFM analysis on DAAm- and IBA-based resin formulations under UV exposure (Fig. 4). The top row (Panels A–C) presents DAAm-based samples at progressively higher magnifications, each revealing uniform, spherical domains characteristic of well-defined PISA nanostructures. In contrast, the bottom row (Panels D–F) shows vesicle-like features in an IBA-based resin formulated at DP 500 and 45 wt% solids. Although these IBA samples produced distinct vesicular morphologies in AFM, the material did not cure to form stable 3D objects and remained partially liquid post-UV irradiation. In separate work, however, an IBA-based resin at a lower target degree of polymerization (DP 125) and 40 wt% solids was successfully cured into solid structures. Moreover, previous studies[11] have shown that acrylamide-based (AM) resins can yield an array of morphologies, including nano-spheres and worm-like micelles, underscoring the versatility of PISA formulations for tuning polymer architectures through appropriate monomer selection, degree of polymerization, and solids content.

The fabrication of perfusable capillary networks remains critical in advancing tissue engineering and regenerative medicine, as efficient nutrient transport and waste removal within engineered tissues depend on precise and reliable vascular architectures. Conventional bioprinting approaches, such as extrusion-based techniques, typically rely on slow, sequential deposition processes, limiting their throughput, resolution, and mechanical stability. In response, we have explored the MCFS-based PISA printing approach to rapidly produce intricate, perfusable vascular structures with controlled dissolution and mechanical properties.

Building upon the nanoscale morphological insights obtained from AFM imaging (Fig. 4), we evaluated the practical applicability of our MCFS-based printing method by fabricating three-dimensional perfusable capillary networks, as illustrated in Fig. 5. Our CAD-based design strategy (Fig. 5A) incorporates three distinct layers: top and bottom structural layers composed of HEAM crosslinked with 1 wt% MBAC, and an intermediate AM/HEAM (50/50 molar ratio) sacrificial layer without crosslinker that forms the microcapillary channels. During printing, the top structural layer is deliberately over-cured so that only rectangular solvent-access wells remain open, facilitating selective dissolution of the underlying fugitive resin.

Fig. 5B and C show printed parts immediately after the second (fugitive) layer is laid down and upon completion of all

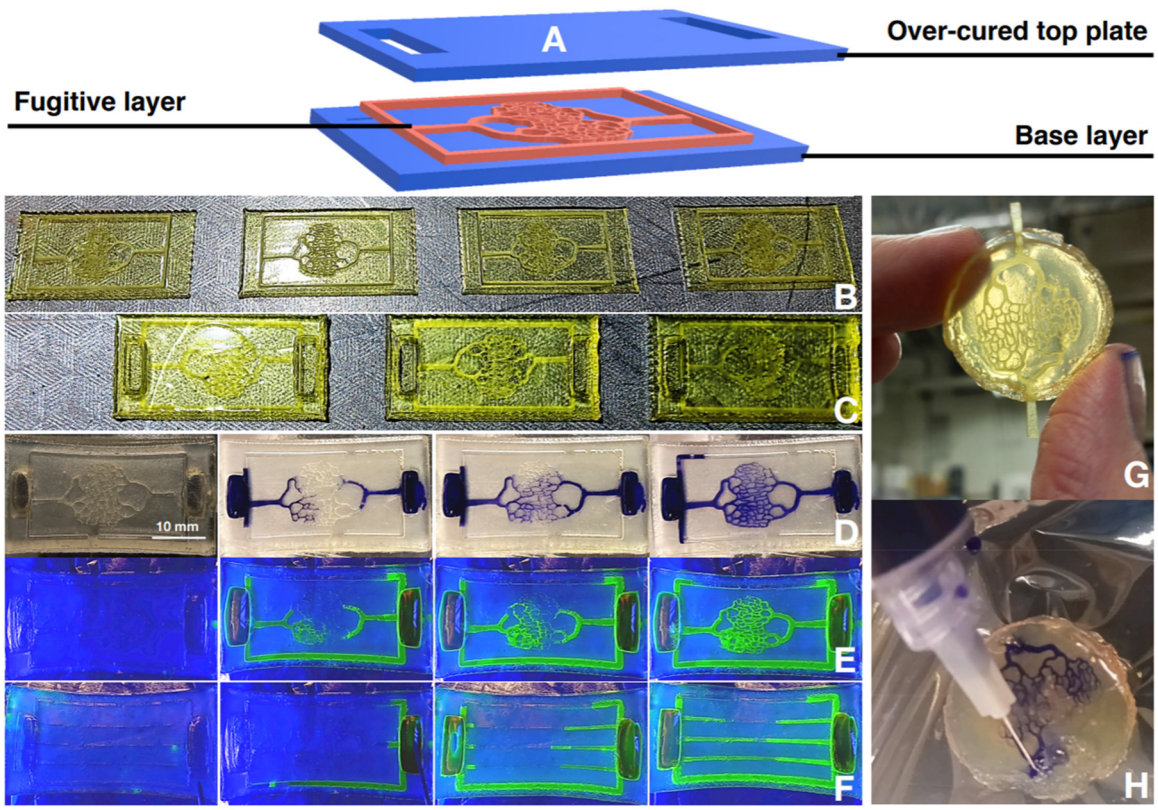

Fig. 5 Three-layer printing and microcapillary perfusion validation. (A) CAD schematic of the three-layer printing design. (B) Printed structure after completion of the base and fugitive layers. (C) Fully printed three-layer structure immediately after fabrication. (D) Microcapillary perfusion test with a blue dye solution. (E) Microcapillary perfusion with fluorescein. (F) Parallel microchannels printed and perfused with fluorescein. (G) DAAM filaments embedded within a GelMA matrix prior to dissolution. (H) Perfusion of the resulting open channel after DAAM removal, confirming the functional integrity of the printed construct. Scale bars are shown where applicable.

three layers, respectively. Selective removal of the intermediate layer is performed by immersing the constructs in distilled water. The resulting hollow microcapillaries are perfused with aqueous dyes: a blue dye is shown in Fig. 5D, while fluorescein perfusion is demonstrated in Fig. 5E. In a parallel setup (Fig. 5F), we patterned and perfused multiple parallel channels with fluorescein, confirming the reproducibility of this approach.

For additional versatility, an alternative fabrication route incorporated DAAM filaments into a gelatin methacrylate (GelMA) hydrogel (Fig. 5G). After UV curing of the GelMA matrix, the DAAM filaments were dissolved with DMSO, generating well-defined channels that were subsequently perfused (Fig. 5H). These constructs showed sufficient mechanical stability for handling while maintaining open, functional channels. Together, these results highlight the adaptability of our MCFS-based PISA printing technique for generating high-resolution, mechanically robust, and perfusable structures that hold promise for a wide range of biomedical and tissue engineering applications.

Polydimethylsiloxane (PDMS) is widely utilized in microfluidics, organ-on-a-chip devices, and biomedical engineering due to its transparency, flexibility, biocompatibility, and ease of processing. However, conventional PDMS microfluidic fabrication relies primarily on soft lithography, which requires complex photolithographic mold preparation and limits rapid prototyping and design flexibility. To address these limitations, we employed our MCFS-based PISA printing method to fabricate sacrificial molds for creating open-channel PDMS microstructures *via* thiol–ene photopolymerization (Fig. 6).

As shown in Fig. 6 (top), sacrificial acrylamide-based molds were printed directly onto the build plate using predefined CAD designs, consisting of cylindrical pillars enclosed by rectangular walls. PDMS matrices were then formed by casting a solution containing divinyl PDMS, thiolated PDMS, and TPO initiator dissolved in MEK onto the printed molds. The PDMS formulation was rapidly cured through thiol–ene photopolymerization upon brief exposure to 405 nm UV irradiation. Following curing, selective dissolution of the acrylamide-based molds was achieved by overnight immersion in distilled water, resulting in open cylindrical channels within robust PDMS matrices.

The resulting PDMS microstructures exhibited well-defined cylindrical channels, with measured dimensions ranging from approximately 128 μm to 497 μm, closely matching the original CAD designs. Optical microscopy images and close-up photographs confirmed successful mold removal, open channel formation, and high structural fidelity. These results illustrate that combining our MCFS-based PISA printing approach with

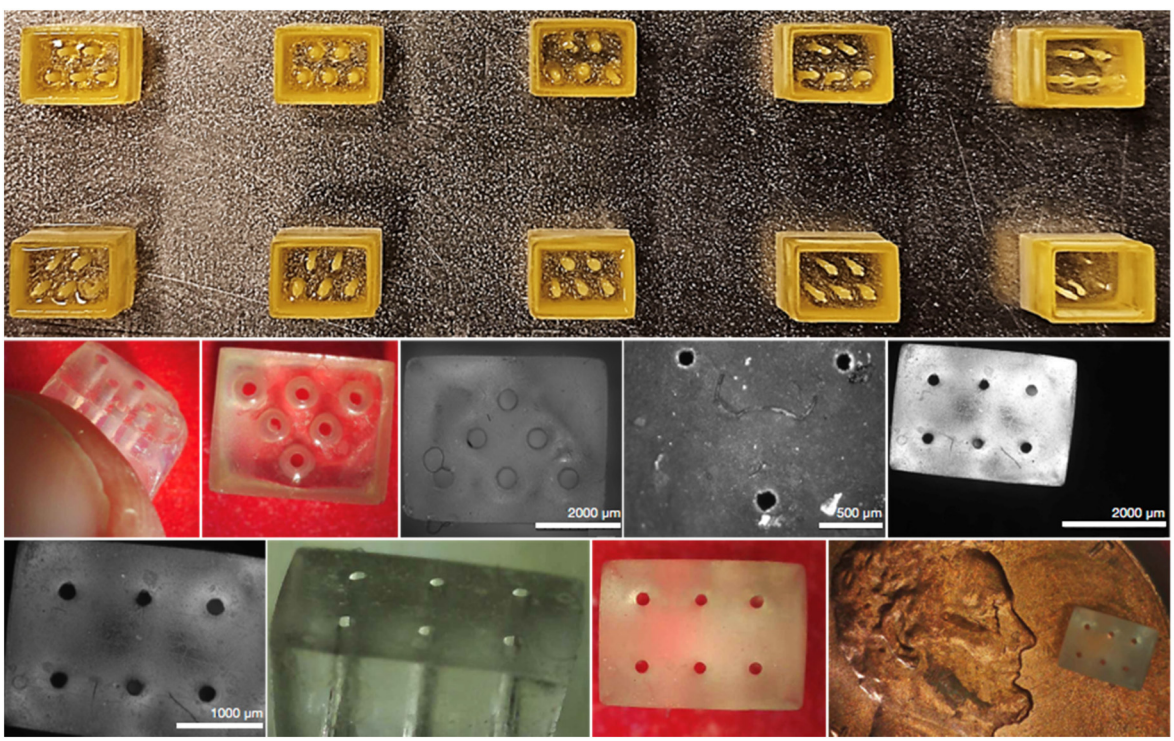

Fig. 6 Fabrication of open-channel PDMS microstructures using printed sacrificial molds. (Top) Photograph showing an array of acrylamide-based sacrificial molds directly printed onto the build plate, each consisting of five to six cylindrical pillars enclosed within rectangular walls. (Bottom) Corresponding PDMS matrices formed by casting and UV-curing a thiol–ene resin formulation composed of 66.7 wt% divinyl PDMS, 33.3 wt% thiolated PDMS, and 1 wt% TPO initiator dissolved in butyl acetate. After selective dissolution of the acrylamide molds overnight in distilled water, well-defined cylindrical channels remained within the robust PDMS matrices. Optical microscopy and close-up images confirm successful mold removal and reveal channel dimensions ranging from approximately 128 μm to 497 μm, accurately reflecting the original CAD designs. Scale bars are provided for reference.

thiol–ene photochemistry enables rapid, flexible, and precise fabrication of intricate PDMS-based microfluidic platforms. This methodology significantly simplifies the prototyping process for organ-on-a-chip devices, enabling rapid exploration of complex, customized microfluidic architectures for biomedical and bioengineering applications.

Conclusions

In summary, we presented a simplified, one-pot approach for synthesizing multi-CTA functional scaffolds (MCFS), significantly streamlining PISA-based multi-material printing by using commercially available reagents without requiring additional purification or conjugation steps. This method enables precise control over nanoscale morphologies and selective dissolution behaviors, facilitating rapid fabrication of intricate, perfusable microchannel networks with high structural fidelity. The approach was successfully applied to create mechanically robust microfluidic devices, including open-channel PDMS structures fabricated *via* sacrificial molds and thiol–ene photopolymerization. Overall, our MCFS-based PISA printing strategy offers a versatile and accessible toolset for rapid prototyping of microstructured devices relevant to tissue engineering and organ-on-a-chip applications.

Data availability

All data supporting the findings of our manuscript titled "PISA Printing Perfusable Microcapillaries" are included within the article itself and its ESI.† Additional datasets generated and/or analyzed during this study, including detailed experimental procedures, synthesis methods, and analytical results, are available from the corresponding author upon reasonable request.

We affirm our commitment to providing all necessary data to support transparency and reproducibility in our research.

Conflicts of interest

There are no conflicts of interest to declare.

Acknowledgements

We would like to acknowledge the Center for Biomedical Research (CBR) at Missouri University of Science and Technology for seed funding.

References

1 S. V. Murphy and A. Atala, *Nat. Biotechnol.*, 2014, **32**, 773–785.
2 K. Liang, *Bioengineering*, 2023, **10**, 1400.
3 L. Ouyang, R. Yao, Y. Zhao and W. Sun, *Biofabrication*, 2016, **8**, 035020.
4 J. R. Tumbleston, D. Shirvanyants, N. Ermoshkin, R. Janusziewicz, A. R. Johnson, D. Kelly, K. Chen, R. Pinschmidt, J. P. Rolland, A. Ermoshkin, E. T. Samulski and J. M. DeSimone, *Science*, 2015, **347**, 1349–1352.
5 Y. Bao, N. Paunović and J.-C. Leroux, *Adv. Funct. Mater.*, 2022, **32**, 2109864.
6 M. J. Derry, L. A. Fielding and S. P. Armes, *Prog. Polym. Sci.*, 2016, **52**, 1–18.
7 S. Perrier, *Macromolecules*, 2017, **50**, 7433–7447.
8 N. J. Warren and S. P. Armes, *J. Am. Chem. Soc.*, 2014, **136**, 10174–10185.
9 J. R. Lovett, N. J. Warren, L. P. D. Ratcliffe, M. K. Kocik and S. P. Armes, *Angew. Chem., Int. Ed.*, 2015, **54**, 1279–1283.
10 A. Priester, J. Yeng, Y. Zhang, R. Wang and A. J. Convertine, *RSC Appl. Polym.*, 2024, **2**, 612–623.
11 A. Priester, J. Yeng, Y. Zhang, K. Hilmas, R. Wang and A. J. Convertine, *ACS Appl. Polym. Mater.*, 2024, **6**, 1944–1950.
12 A. Priester, J. Yeng, Y. Zhang, R. Wang and A. J. Convertine, *Polym. Chem.*, 2023, **14**, 2452–2456.
13 J. Vajda, M. Milojević, U. Maver and B. Vihar, *Biomedicines*, 2021, **9**, 589.
14 R. Hooper, C. Cummings, A. Beck, J. Vazquez-Armendariz, C. Rodriguez and D. Dean, *Biofabrication*, 2024, **16**, 025032.
15 D. B. Kolesky, K. A. Homan, M. A. Skylar-Scott and J. A. Lewis, *Proc. Natl. Acad. Sci. U. S. A.*, 2016, **113**, 3179–3184.
16 B. Grigoryan, S. J. Paulsen, D. C. Corbett, D. W. Sazer, C. L. Fortin, A. J. Zaita, P. T. Greenfield, N. J. Calafat, J. P. Gounley, A. H. Ta, F. Johansson, A. Randles, J. E. Rosenkrantz, J. D. Louis-Rosenberg, P. A. Galie, K. R. Stevens and S. J. Miller, *Science*, 2019, **364**, 458–464.
17 E. M. Maines, M. K. Porwal, C. J. Ellison and T. M. Reineke, *Green Chem.*, 2021, **23**, 6863–6897.
18 H. Gojzewski, Z. Guo, W. Grzelachowska, M. G. Ridwan, M. A. Hempenius, D. W. Grijpma and G. J. Vancso, *ACS Appl. Mater. Interfaces*, 2020, **12**, 8908–8914.
19 J. Li, C. Boyer and X. Zhang, *Macromol. Mater. Eng.*, 2022, **307**, 2200021.
20 Z. Zhang, N. Corrigan, A. Bagheri, J. Jin and C. Boyer, *Angew. Chem., Int. Ed.*, 2019, **58**, 17954–17963.
21 M. Semsarilar and V. Abetz, *Macromol. Chem. Phys.*, 2020, **222**, 2000311.
22 C. Gao, S. Li, Q. Li, P. Shi, S. A. Shah and W. Zhang, *Polym. Chem.*, 2014, **5**, 6957–6966.
23 A. Bagheri, K. E. Engel, C. W. A. Bainbridge, J. Xu, C. Boyer and J. Jin, *Polym. Chem.*, 2020, **11**, 641–647.
24 B. Zhao, J. Li, Y. Xiu, X. Pan, Z. Zhang and J. Zhu, *Macromolecules*, 2022, **55**, 1620–1628.
25 T. Maruyama, M. Mukai, R. Sato, M. Iijima, M. Sato, T. Furukawa and S. Maruo, *ACS Appl. Polym. Mater.*, 2022, **4**, 5515–5523.
26 X. Shi, J. Zhang, N. Corrigan and C. Boyer, *Mater. Chem. Front.*, 2021, **5**, 2271–2282.

27 P. Blais, P. Beaunier, F. Stoffelbach and J. Rieger, *Polym. Chem.*, 2018, **9**, 4483–4491.
28 S. L. Canning, G. N. Smith and S. P. Armes, *Macromolecules*, 2016, **49**, 1985–2001.
29 N. J. W. Penfold, J. Yeow, C. Boyer and S. P. Armes, *ACS Macro Lett.*, 2019, **8**, 1029–1054.
30 J. Wan, B. Fan and S. H. Thang, *Chem. Sci.*, 2022, **13**, 4192–4224.
31 M. Markovic, J. Van Hoorick, K. Hölzl, M. Tromayer, P. Gruber, S. Nürnberger, P. Dubruel, S. Van Vlierberghe, R. Liska and A. Ovsianikov, *J. Nanotechnol. Eng. Med.*, 2015, **6**, 021001.
32 R. Suntornnond, E. Y. S. Tan, J. An and C. K. Chua, *Sci. Rep.*, 2017, **7**, 16902.
33 Q. Gao, Z. Liu, Z. Lin, J. Qiu, Y. Liu, A. Liu, Y. Wang, M. Xiang, B. Chen, J. Fu and Y. He, *ACS Biomater. Sci. Eng.*, 2017, **3**, 399–408.